Influence of Co layer thickness on the structural and magnetic properties of multilayers

A Zarefy, L Lechevallier, R Lardé, H Chiron, J-M Le Breton, V Baltz, B Rodmacq, B Dieny

▶ **To cite this version:**

HAL Id: hal-00569614
https://hal.archives-ouvertes.fr/hal-00569614

Submitted on 25 Feb 2011

Influence of Co layer thickness on the structural and magnetic properties of (Pt/Co$_{tCo}$)$_3$/Pt$_{tPt}$/IrMn multilayers

A Zarefy[1], L Lechevallier[1], R Lardé[1], H Chiron[1], J-M Le Breton[1], V Baltz[2], B Rodmacq[2] and B Dieny[2]

[1]Groupe de Physique des Matériaux, UMR CNRS 6634, Université de Rouen

Avenue de l'Université BP 12, 76801 Saint Etienne du Rouvray, France

[2]SPINTEC (UMR 8191 CEA-CNRS-UJF- Grenoble INP)

CEA/INAC, 38054 Grenoble Cedex 9, France

E-mail: luc.lechevallier@univ-rouen.fr

Abstract

The correlated effects of the insertion of a Pt spacer between ferromagnetic and antiferromagnetic layers and of the variation of the Co layers thickness on the structural and magnetic properties of [(Pt/Co$_{tCo}$)$_3$/Pt$_{tPt}$/IrMn]$_n$ multilayers have been studied. Samples with n = 1 and 7, t$_{Co}$ = 0.4 and 0.6 nm, t$_{Pt}$ = 0 and 0.4 nm have been investigated by tomographic atom probe and superconducting quantum interference device magnetometry. For spacer free samples (t$_{Pt}$ = 0), the structural investigation shows that when t$_{Co}$ = 0.4 nm, Mn and Ir atoms diffuse deeply in the (Pt/Co) multilayers. In contrast for t$_{Co}$ = 0.6 nm, the Mn and Ir diffusion is much reduced. Because Pt acts as a barrier against the Mn and Ir diffusion, this difference is less pronounced in samples with Pt insertion. The hysteresis loops shapes, the exchange bias fields and the saturation magnetization values were correlated with the structural properties of these samples and discussed, taking into account the susceptibility, exchange stiffness, and perpendicular magnetic anisotropy.

Corresponding author: Dr Luc Lechevallier

Groupe de Physique des Matériaux

UMR 6634 CNRS, Université de Rouen

Site universitaire du Madrillet

avenue de l'Université, BP 12

76801 Saint Etienne du Rouvray Cedex, France

tel : 33 (0) 2-32-95-51 25

fax : 33 (0) 2-32-95-50-32

E-mail: luc.lechevallier@univ-rouen.fr

1. Introduction

In ferromagnetic/antiferromagnetic bilayers, the phenomenon of exchange bias, which refers to the shift of the hysteresis loop along the magnetic field axis direction (H_E) and to the enhancement of the coercivity (H_C), originates from exchange interactions between ferromagnetic (FM) and antiferromagnetic (AFM) layers. Optimum loop shift is obtained after field cooling from above the blocking temperature of the AFM layer or after deposition under the presence of a magnetic field [1-6]. During the last decade, these systems have been extensively investigated due to their applications in the development of spintronic devices, such as spin valve and tunnel junctions [7-9].

In most cases, the exchange bias effect has been observed in FM/AFM layers with in-plane anisotropy [3]. However, few years ago, exchange bias with perpendicular anisotropy in multilayers has also been investigated [9-13] offering the possibility to develop spin valves or tunnel junctions with perpendicular to plane magnetization [14,15]. Among these systems $(Pt/Co)_n$ FM multilayers exchange coupled to an AFM layer, such as IrMn or FeMn, have been intensively studied. The perpendicular anisotropy of these FM multilayers depends on several parameters, such as the number of (Pt/Co) repeats, n, or the thickness of the Co and Pt layers [15-17]. Sort et al. showed that in $(Pt/Co)_n/IrMn$ structures, for a fixed number of (Pt/Co) repeats, the exchange bias field H_E and the coercive field H_C can be strongly modified by varying the Co layer thickness (t_{Co}) [15]. It has been also observed that the largest perpendicular effective anisotropy is obtained for intermediate values of t_{Co}, between 0.6 and 0.9 nm [15,18-20].

In addition, it has been shown that, for a low value of t_{Co} (0.4 nm), a strong increase of H_E and H_C fields can be obtained by introducing an ultrathin Pt layer between the $(Pt/Co)_n$ multilayer and the IrMn layer [14,15,21,22]. This has been ascribed to the reinforcement of the perpendicular orientation of the topmost Co magnetization by the introduction of an additional Co/Pt interface [15,23], which prevails over the FM and AFM magnetic decoupling induced by the Pt insertion. Recently, we have shown that in $(Pt/Co_{0.4nm})_3/Pt_{tPt}/IrMn$ multilayers, the Pt spacer also acts as a diffusion barrier, which prevents Mn diffusion into the Co layer in contact with IrMn and thereby also contributes to the reinforcement of the perpendicular anisotropy [24]. In the $t_{Co} = 0.6$ nm samples, the introduction of a

Pt spacer between the $(Pt/Co)_n$ multilayer and the IrMn layer does not lead to an increase of H_E [15] but, on the contrary, to a strong decrease, showing thus a very different behaviour from the $t_{Co} = 0.4$ nm samples. For $t_{Co} = 0.6$ nm, the magnetic decoupling induced by the Pt insertion seems to prevail over the interfacial anisotropy enhancement. It thus appears that the role of the Pt spacer depends on the adjacent Co layers thickness.

In this work, we investigate $(Pt/Co_{tCo})_3/Pt_{tPt}/IrMn$ multilayers, in order to study the combined influence of a Pt spacer insertion ($t_{Pt} = 0$ and 0.4 nm) at the FM/AFM interface and of the Co layers thickness ($t_{Co} = 0.4$ and 0.6 nm) on their chemical, structural and magnetic properties. We used Laser Assisted Tomographic Atom Probe (LATAP) to characterize the structure of these multilayers at the atomic scale. We correlated the structural results with the exchange bias field values (H_E), the saturation magnetization (M_s) and the shape of the hysteresis loops, as measured by SQUID magnetometry at 5 K and 300 K for one and seven repeats of the $(Pt/Co_{tCo})_3/Pt_{tPt}/IrMn$ sequence, in order to explain the different magnetic behaviour of the $t_{Co} = 0.4$ and 0.6 nm samples.

2. Experimental – samples preparation

The $Ta_{3nm}/[(Pt_{2nm}/Co_{tCo})_3/Pt_{tPt}/IrMn_{7nm}]_n/Pt_{10nm}$ multilayers with $t_{Co} = 0.4$ and 0.6 nm, $t_{Pt} = 0$ and 0.4 nm, and with n = 1 and 7 were deposited by DC magnetron sputtering at room temperature, using a 5.3×10^{-6} Pa base pressure and a 0.25 Pa Ar pressure during deposition. The samples were subsequently annealed at 550 K (*i.e.* above the blocking temperature of the AFM layer) in another vacuum chamber using a 10^{-4} Pa pressure and cooled under a - 2.4 kOe field applied perpendicular to the film plane (*i.e.* sufficient to saturate the FM multilayer) in order to set the unidirectional exchange anisotropy towards this direction.

All multilayers were deposited onto Si/SiO_2 substrates for SQUID magnetic characterizations. For n = 7, the multilayers were additionally deposited onto pre-patterned substrates consisting of an assembly of flat-topped Si (100) posts in order to perform the Atom Probe analysis [25]. These substrates with posts of 100 μm height and 10×10 μm^2 area were obtained after patterning of Si wafer by a Bosch process [26]. The atom probe technique counts, chemically identifies and spatially locates

4

individual atoms using the basic principles of field evaporation of surface atoms from a sample prepared in the form of sharp needles, with an end radius less than 50 nm [24,27,28]. The evaporated atoms are collected by a time-resolved position detector located in front of the specimen. It allows to measure the time of flight of each ion and to record its impact position. These combined information allow to deduce the chemical nature of evaporated ions and to calculate the position from which atoms originate at the tip surface. This allows obtaining the 3D reconstruction of the analyzed volume and thus, the observation of the spatial distribution of atoms at the atomic scale in real space [29]. From these data, chemical composition or concentration depth profiles can be calculated everywhere in the analysed volume. The depth resolution is better than half an atomic plane [28].

Tips required for atom probe analysis were prepared using a focused ion beam (FIB) annular milling with a Ga ion beam [25,30]. In order to protect the multilayer from being damaged by the FIB milling during sample preparation, a capping layer of Cr was deposited on the top of the posts. The tips were milled, in a first step with high energy Ga beam (30 keV) and in a second step with a lower energy (2 keV) Ga beam, in order to reduce Ga implantation. Moreover, seven repeats of $(Pt/Co_{tCo})_3/Pt_{tPt}/IrMn$ sequence were deposited in order to obtain a sufficient thickness of samples allowing a perfect characterisation of the interfaces in regions undamaged by Ga ions. Prepared tips were then analysed by LATAP at 80 K in an ultrahigh vacuum chamber at a 10^{-8} Pa pressure.

The magnetic properties of the multilayers were characterized by using a superconducting quantum interference device magnetometer (SQUID). The hysteresis loops were measured at room temperature and 5 K with the magnetic field applied perpendicularly to the film plane. From room temperature to 5 K, the samples were field cooled under an out-of-plane saturating magnetic field.

3. Results and discussion

3.1. Structural characterization by LATAP

Samples containing seven repeats of the $(Pt/Co_{tCo})_3/Pt_{tPt}/IrMn$ sequence with $t_{Co} = 0.4$ and 0.6 nm, $t_{Pt} = 0$ and 0.4 nm were analyzed by LATAP. Figure 1 shows a 2D projection of the 3D-reconstruction of an analyzed volume representing the spatial distribution of Pt, Co, Ir and Mn atoms

in approximately three sequences of the $[(Pt/Co_{0.6nm})_3/IrMn]_7$ multilayer. The image is oriented in order to show the interfaces in cross section, i.e. perpendicular to the plane of view. In this figure, each point corresponds to one atom. The three Co layers are clearly observable in each sequence, and the IrMn, Co and Pt layers can also be clearly identified. In order to correctly label the layers, the first Pt layer deposited on IrMn is named $Pt_{(1)}$. It is covered during the deposition sequence by the $Co_{(1)}$, $Pt_{(2)}$, $Co_{(2)}$, $Pt_{(3)}$ and $Co_{(3)}$ layers, successively.

The high depth resolution of the technique allows to reveal the atomic planes in the Pt layers which corresponds to the Pt(111) texture. The atomic planes were observed in the three Pt layers of the $(Pt/Co)_3$ multilayer in each sequence. The Pt atomic planes and the estimated thickness of the crystalline zone (deduced from the 0.2266 nm distance between two Pt(111) atomic planes) in one sequence of the $[(Pt/Co_{0.6nm})_3/IrMn]_7$ multilayer are shown in figure 2. For such samples with $t_{Co} = 0.6$ nm, the atomic planes are observable in the $Pt_{(1)}$ layer which is deposited on IrMn while for samples with $t_{Co} = 0.4$ nm, the atomic planes are only observable for the $Pt_{(2)}$ and $Pt_{(3)}$ layers but not for the $Pt_{(1)}$ layer [24]. Thus, a larger Co thickness seems to promote a better texture of the (111) Pt layer and a better crystalline state of the whole sample.

In order to investigate the effect of the Pt spacer on the $(Pt/Co)_3/IrMn$ interface at the atomic scale, for both $t_{Co} = 0.4$ and 0.6 nm, we analyzed one sequence of $[(Pt_{2nm}/Co_{0.4nm})_3/Pt_{tPt}/IrMn_{7nm}]_7$ multilayers by LATAP. For $t_{Co} = 0.4$ nm and without Pt spacer inserted between the $Co_{(3)}$ layer and the IrMn layer ($t_{Pt} = 0$ nm), a strong intermixing between Co and Mn atoms has been previously observed at the Co/IrMn interface [24,28] due to the Mn and Ir atoms diffusion in the whole thickness of the $Co_{(3)}$ layer. However, in the sample with Pt insertion (with $t_{Co} = 0.4$ nm), the Co/Pt/IrMn interface is sharper, as due to the role of the Pt spacer in preventing the Mn and Ir diffusion into the $Co_{(3)}$ layer [24].

For $t_{Co} = 0.6$ nm, figure 3 shows a 2D projection of the 3D-reconstruction corresponding to the spatial distribution of Co and IrMn atoms in one sequence of $[(Pt_{2nm}/Co_{0.6nm})_3/Pt_{tPt}/IrMn_{7nm}]$ multilayers with $t_{Pt} = 0$ nm and $t_{Pt} = 0.4$ nm. One can see that the Co/IrMn interface for $t_{Pt} = 0$ nm is weakly intermixed, due to the diffusion of Mn and Ir atoms in the $Co_{(3)}$ layer of the $(Pt/Co)_3$ multilayer (figure 3(a)). For $t_{Pt} = 0.4$ nm, the Co/Pt/IrMn interface appears to be sharper. As for $t_{Co} = 0.4$ nm

6

samples [24], the Pt spacer inserted between IrMn layer and $(Pt/Co)_3$ multilayer prevents from the Mn and Ir diffusion into the $Co_{(3)}$ layer. It is clearly observed in figure 3(b) that IrMn and $Co_{(3)}$ layers are well separated.

Figure 4 shows a 2D projection of the 3D-reconstruction corresponding to the spatial distribution of Co and IrMn atoms in one sequence of a $[(Pt_{2nm}/Co_{tCo})_3/IrMn_{7nm}]$ multilayer (without Pt spacer), for t_{Co} = 0.4 and 0.6 nm. This figure allows to compare the extent of the Ir and Mn atoms diffusion in the $Co_{(3)}$ layer in samples with different Co thicknesses. For the t_{Co} = 0.6 nm sample, the Mn and Ir atoms diffused through half of the $Co_{(3)}$ layer whereas for t_{Co} = 0.4 nm, the intermixing zone extends further *i.e.* throughout the entire thickness of the $Co_{(3)}$ layer.

Figures 5(a) and 5(b) present the concentration profiles of one sequence of a $[(Pt/Co_{0.6nm})_3/Pt_{tPt}/IrMn]_7$ multilayer for t_{Pt} = 0 and 0.4 nm respectively, corresponding to the analyzed volume in figure 3. Figures 5(c) and 5(d) are the enlargements of figures 5(a) and 5(b) in the (Pt/Co)/IrMn interfacial zone, respectively. For the sake of clarity, the Ir profile, which is connected to the Mn one, is not represented

It can be observed in figure 5(a) and more clearly in figure 5(c) that, for t_{Pt} = 0 nm, the Co atoms in $Co_{(3)}$ layer are intermixed with Mn and Pt atoms. Mn atoms enter the $Co_{(3)}$ layer with a concentration close to 10 at.% in the middle of the $Co_{(3)}$ layer (maximum Co concentration being 60 at.%). In figure 5(b) and figure 5(d), for the t_{Pt} = 0.4 nm sample, a small Pt peak corresponding to the Pt spacer is observed. It clearly appears that the Mn concentration decreases when the Pt concentration increases and is low in the whole $Co_{(3)}$ layer thickness. Moreover, the Mn concentration in the middle of the $Co_{(3)}$ layer is close to 5 at.% in the t_{Pt} = 0.4 nm sample. It is slightly lower than in the t_{Pt} = 0 nm sample. This clearly demonstrates the role of Pt as a diffusion barrier for Ir and Mn.

Figures 6(a) and 6(b) show the Pt, Co and Mn concentration profiles, corresponding to the $(Pt/Co_{tCo})/IrMn$ interfacial zone, for the t_{Co} = 0.4 and 0.6 nm samples, respectively, both with t_{Pt} = 0 nm. One clearly sees that the Mn atoms penetrate into the $Co_{(3)}$ layer in both cases. For the t_{Co} = 0.4 nm sample, the Mn atoms diffuse into the whole thickness of the Co layer with a concentration of 20 at.% in the middle of the $Co_{(3)}$ layer for which the maximum concentration is close to 50 at.%. For the t_{Co} = 0.6 nm sample, the thickness of the $Co_{(3)}$ layer being larger than in the previous case, the Mn atoms

diffusion is limited approximately at the half of the $Co_{(3)}$ layer, with a Mn concentration of 10 at.% in the middle of the $Co_{(3)}$ layer (maximum Co concentration being 60 at.%). Consequently, in these two spacer free samples, it clearly appears that the $Co_{(3)}$ layer is less intermixed in the $t_{Co} = 0.6$ nm sample than in the $t_{Co} = 0.4$ nm sample. The Mn diffusion depth seems to be longer in the the $t_{Co} = 0.4$ nm sample than in the $t_{Co} = 0.6$ nm sample. This could be explained by the stress induced by the adjacent $Pt_{(3)}$ layer on the $Co_{(3)}$ layer. The interfacial stress and related impact on the Co lattice cell is certainly more important for the thinner Co layer. This may favour the Mn and Ir diffusion within this layer. The relative impact of the Mn diffusion in the $Co_{(3)}$ layer is thus even more important for the $t_{Co} = 0.4$ nm sample than for the $t_{Co} = 0.6$ nm one.

In the samples with Pt insertion, the effect of the Pt spacer, acting as a diffusion barrier against the Mn and Ir diffusion in the $Co_{(3)}$ layer, is consequently less determining for the $t_{Co} = 0.6$ nm sample than for the $t_{Co} = 0.4$ nm sample.

3.2. Magnetic properties

The four samples containing seven repeats present bottom $Co/Pt_{tPt}/IrMn$ interfaces but also top $IrMn/Pt_{2nm}/Co$ ones [31]. Given the large thickness (2 nm) of the Pt spacer for the top interface [15], we can reasonably assume that the exchange bias interaction is only due to the bottom $Co/Pt_{tPt}/IrMn$ interface.

Hysteresis loops of all samples, as measured at room temperature and at 5 K are shown in figures 7 and 8. Saturation magnetization measurements M_S of these samples, at 5 K and room temperature, deduced from the hysteresis loops are given in Table 1. The error in the values of M_S is estimated to ±5%. The resolution of the SQUID is 10^{-8} emu, which is well below the signals of around 2×10^{-5} emu at saturation from all of our samples. The error on the M_S values in emu.cm^{-3} is thus mainly due to the error on the estimation of the volume of our samples, which we calculate to be ±5%.

At 5 K, for n = 7 and $t_{Pt} = 0.4$ nm samples (samples with Pt insertion), the M_S values are similar for $t_{Co} = 0.4$ nm and $t_{Co} = 0.6$ nm samples (1474 and 1458 emu.cm^{-3}) and close to the M_S of bulk Co (1400 emu.cm^{-3}). This confirms that for the two Co thicknesses, there is very limited intermixing at the FM/AFM interface susceptible to decrease M_S of the Co layers, in agreement with

LATAP analysis. The fact that M_S is slightly higher than that of bulk Co can be ascribed to the error bars in the M_S measurement or to a probable Pt polarization (Pt layers in contact with Co layers) as already observed and measured [32].

In contrast to the previous remark, at 300 K and for the same samples, the M_S values are different for t_{Co} = 0.4 nm and t_{Co} = 0.6 nm samples, (1025 and 1208 emu.cm^{-3}, respectively). The M_S value of the t_{Co} = 0.4 nm sample is lower than in the t_{Co} = 0.6 nm sample. This is independent of inter-diffusion effects at the FM/AFM interface because there is only very limited inter-diffusion for the samples with Pt insertion, as previously reminded. This is due to the fact that the Curie temperature (T_C) of the t_{Co} = 0.4 nm sample is lower than that of t_{Co} = 0.6 nm sample [33] so that at room temperature, the reduction of magnetization due to thermally activated excitations is larger in the t_{Co} = 0.4 nm sample than in its t_{Co} = 0.6 nm counterpart.

At 5 K for n = 7 and t_{Co} = 0.4 nm, the reduction of the M_S value for the spacer free sample compared to that of the sample with Pt insertion, from 1474 to 1262 emu.cm^{-3} can be ascribed to the presence of a strong intermixing for the spacer free sample, as evidenced in the LATAP measurements [24]. At 300 K and for these two samples, the relative difference between the M_S values is close to 25 % (1025 for t_{Pt} = 0.4 nm to 765 emu.cm^{-3} for t_{Pt} = 0 nm) which is higher than that obtained at 5 K, close to 14 % (1474 for t_{Pt} = 0.4 nm to 1262 emu.cm^{-3} for t_{Pt} = 0 nm). In the case of the spacer free sample, it is likely that the inter-diffusion leads to an additional decrease of T_C as well known in CoMn alloys of increasing Mn content [34]. It results that as the temperature increases, M_S decreases faster for the spacer free sample than for the sample with Pt insertion. The difference between the M_S values in these two types of samples at 300 K can therefore be ascribed to the impact of inter-diffusion on M_S as well as on T_C.

At 5 K for n = 7 and t_{Co} = 0.6 nm, the reduction of the M_S value for the spacer free sample, from 1458 to 1296 emu.cm^{-3} can also be ascribed to the presence of a slight inter-diffusion for the spacer free sample. However, the difference between the two M_S values, here close to 11 % is smaller than in the previous case (14 %) and can be the result of a lower inter-diffusion in the t_{Co} = 0.6 nm spacer free sample than in the t_{Co} = 0.4 nm spacer free sample, as shown by LATAP analysis.

For n = 7 and t_{Pt} = 0 nm (samples without spacer), the M_S decrease when the temperature increases from 5 K to 300 K is more important for the t_{Co} = 0.4 nm sample (from 1262 to 765 emu.cm^{-3}, i.e. 39 %) than for the t_{Co} = 0.6 nm sample (from 1296 to 1093 emu.cm^{-3}, i.e. 16 %). This can be ascribed to a lower Curie temperature in the t_{Co} = 0.4 nm sample than in the t_{Co} = 0.6 nm one due to both an intrinsic influence of a reduced Co thickness (larger role of thermal fluctuations) and larger Mn diffusion into the Co layer for the thinner Co layer. This is again consistent with a lower Mn diffusion in the $Co_{(3)}$ layer for the t_{Co} = 0.6 nm sample than for the t_{Co} = 0.4 nm sample.

The differences between the values for n = 7 and n = 1 are well within the error bars. The values and trends of the saturation magnetization as measured for n = 1 confirm those for n = 7.

The values of H_E as extracted from figures 7 and 8 are given in Table 2. H_E being inversely proportional to the thickness t_{FM} and the saturation magnetization M_S of the FM layer, we could expect, taking into account the smaller t_{FM} and M_S values for the t_{Co} = 0.4 nm samples, higher H_E values for the t_{Co} = 0.4 nm samples than for the t_{Co} = 0.6 nm samples. And yet, it is not what we observed. Thus, for t_{Pt} = 0 nm, the H_E values are higher for the t_{Co} = 0.6 nm samples than for the t_{Co} = 0.4 nm samples. Moreover, the effect of a Pt spacer on H_E is different according to the Co layer thickness of the samples. One can also notice that the H_E values are higher for the samples containing one repeat of the $(Pt/Co_{t_{Co}})_3/Pt_{t_{Pt}}/IrMn$ sequence than for the samples containing seven repeats. Table 2 and figures 7 and 8 show that the insertion of a Pt spacer for one or seven repeats increases H_E for the t_{Co} = 0.4 nm samples but decreases H_E for the t_{Co} = 0.6 nm samples. The large diffusion of Ir and Mn atoms in the $Co_{(3)}$ layer for the t_{Co} = 0.4 nm samples (without spacer), as shown in the structural properties (figures 4 and 6) strongly decreases the anisotropy of the Co atoms of the $Co_{(3)}$ layer and consequently the exchange bias field, H_E [15]. This does not happen in the t_{Co} = 0.6 nm samples (without spacer), the diffusion of Ir and Mn atoms in the $Co_{(3)}$ layer remaining very limited, as shown in figures 4 and 6. Thus, the exchange bias field effect is strong and H_E value is high. Inserting a Pt spacer in the t_{Co} = 0.6 nm samples disrupts the exchange interaction between the Co and Mn ions, thus decreasing the perpendicular magnetic coupling between Co and Mn spins and correlatively H_E. This behaviour is explained by the three-fold role of the Pt spacer, i.e. it strengthens the perpendicular

orientation of the Co magnetization [15] and acts as a barrier to the inter-diffusion of species [24], but it also tends to reduce the exchange bias due to the short-range character of the FM-AFM interactions.

It can also be observed that the hysteresis loops of the four samples containing seven repeats of the $(Pt/Co_{tCo})_3/Pt_{tPt}/IrMn$ sequence (figures 7, 8 (c) and 8 (d)) are slanted whereas those containing one repeat display square hysteresis loops (figures 7, 8 (a) and 8 (b)).

It is known that the magnetization reversal of a magnetic layer with out-of-plane anisotropy strongly depends on its thickness [35-36]. Gehanno et al [37] have shown that the equilibrium susceptibility of such layer decreases exponentially as the thickness of the magnetic layer is increased, as a result of a balance between magnetostatic energy and domain wall energy. This effect can also be treated in terms of a critical film thickness above which the single domain magnetic configuration no more prevails over the multidomain one [35,36,38]. The influence of magnetic domains and the shape of hysteresis loops are taken into account in the expression of the susceptibility χ. Indeed, It has been shown for a single layer that the zero field susceptibility χ versus saturation magnetization M_S, exchange stiffness A, perpendicular anisotropy constant K_u, and film thickness t is approximately given by the relation [37,39]:

$$\chi \approx \frac{(AK_u)^{1/2}}{tM_S^2} + \ln(4) - 1 + \mu(\frac{1}{2} - \ln(2)) \quad \text{With} \quad \mu = (1 + \frac{2\pi M_s^2}{K_u}) \qquad (1)$$

In the case of samples showing a strong perpendicular anisotropy, $K_u > 2\pi M_S^2$, χ mainly depends on the first term of equation (1). In hysteresis loops, the smaller the susceptibility the more slanted the loops are. Thus according to equation (1), if A or K_u increase and M_S remains constant, χ increases resulting in a less slanted loop. In contrast, if A or K_u remain constant and M_S increases, χ decreases and the loop becomes more slanted.

Our present samples can be viewed as seven $(Pt_{2nm}/Co_{tCo})_3$ multilayers separated by $Pt_{tPt}/IrMn_{7nm}$ bilayers, the $(Pt_{2nm}/Co_{tCo})_3$ multilayers being magnetically coupled via magnetostatic energy terms, as detailed in Ref. 40. In the case of $(Pt/Co)_n$ based multilayers similar to ours and separated by a thick Pt spacer (from 4 to 100 nm), it has been shown that inter-$(Pt/Co)_n$ magnetostatic coupling strongly influences the macroscopic magnetization reversal of the whole stack and favours

the formation of a multidomain magnetic configuration. Due to these magnetostatic interactions, the system behaves like a monolayer with increased magnetic effective thickness [29]. Similarly our seven $(Pt_{2nm}/Co_{tCo})_3$ multilayers are magnetostatically coupled via the $Pt_{tPt}/IrMn_{7nm}$ bilayers which also tend to favour the formation of a multidomain magnetic configuration. The whole stack also behaves like a sample with an enhanced magnetic effective thickness. It thus results that for both $t_{Co} = 0.4$ and 0.6 nm, with and without spacer, the magnetic susceptibility for $n = 7$ is lower than the susceptibility for $n = 1$, as observed in figures 7 and 8.

For the samples comprising seven repeats (figures 7, 8 (c) and 8 (d)), it appears that the loops are more slanted for the $t_{Co} = 0.6$ nm samples than for the $t_{Co} = 0.4$ nm samples. This can be first ascribed to the influence of the overall magnetic thickness on the equilibrium susceptibility.

At 300 K for $n = 7$ and $t_{Co} = 0.4$ nm, the LATAP results revealed a strong inter-diffusion in the $t_{Pt} = 0$ nm sample and a much lower inter-diffusion in the $t_{Pt} = 0.4$ nm sample. The addition of the Pt spacer strongly increases K_u as already observed [15]. It also increases M_S (from 765 to 1025 Oe) and T_C (consequently A), as already discussed above. From the observed reduction of χ when the Pt spacer is inserted (figure 7 (c)), it seems that the effect of the M_S increase associated with Pt insertion dominates over the effect of the K_u and A increase.

At 300 K, for $n = 7$ and $t_{Co} = 0.6$ nm, there is a weak inter-diffusion in the $Co_{(3)}$ layer for $t_{Pt} = 0$ nm sample and almost no inter-diffusion for $t_{Pt} = 0.4$ nm sample. The addition of a Pt spacer very slightly modifies K_u, weakly increases M_S and T_C. As a result, the slight increase in M_S is balanced by the increase in A resulting in a weak influence of Pt insertion on χ. This is in agreement with the shape of the loops of two samples (with and without spacer) which are similarly slanted. This remark can also be applied to these two samples at 5 K.

For $n = 7$ and $t_{Co} = 0.6$ nm, the loops are more slanted at 5 K than at 300 K, the slope of the hysteresis loops (calculated around the coercive field) of figure 8 (d) (5 K) and 7 (d) (300 K) being proportional to 1.0×10^{-3} and 1.7×10^{-3} Oe^{-1}, respectively. The susceptibility is thus lower at 5 K than at 300 K. According to the mean field theory, the A thermal variation is proportional to the M_S thermal

variation. K_u weakly varies with temperature. χ being proportional to $(AK_u)^{1/2}/M_S^2$ and M_S increasing when the temperature decreases, it results that χ is indeed expected to be lower at 5 K than at 300 K.

The above explanation also allows us to understand that for n = 7 and t_{Co} = 0.4 nm, the loops are also more slanted at 5 K for the t_{Pt} = 0 and 0.4 nm samples (slope: 1.7×10^{-3}) than at 300 K (slopes: 2.9×10^{-3} and 4.6×10^{-3} Oe^{-1}, for the t_{Pt} = 0.4 and t_{Pt} = 0 nm samples, respectively).

4. Conclusion

The structural investigation of the $Ta_{3nm}/[(Pt_{2nm}/Co_{tCo})_3/Pt_{tPt}/IrMn_{7nm}]_n/Pt_{10nm}$ multilayers (with t_{Co} = 0.4 and 0.6 nm, t_{Pt} = 0 and 0.4 nm, n = 7) by LATAP allowed to accurately characterize the FM/AFM interfaces and to show, at the atomic scale, the structural differences between the t_{Co} = 0.4 nm and t_{Co} = 0.6 nm samples with (or without) a Pt insertion. It appears that in the t_{Co} = 0.4 nm samples, Ir and Mn diffusion leads to more intermixed topmost $Co_{(3)}$ layer than in t_{Co} = 0.6 nm samples. That explains that the insertion of a Pt spacer (which plays the role of a diffusion barrier), between the $Co_{(3)}$ layer and the IrMn layer, has more important effects on magnetic properties in t_{Co} = 0.4 nm samples than in t_{Co} = 0.6 nm samples. The strong intermixing observed at the Co/IrMn interface in the t_{Co} = 0.4 nm samples leads to a significant reduction in exchange bias. In t_{Co} = 0.4 nm samples, the introduction of a Pt spacer prevents the Mn and Ir atoms diffusion in the $Co_{(3)}$ layer. It thus reinforces the out-of-plane orientation of the Co magnetization, leading to an enhancement of both perpendicular magnetic anisotropy and exchange bias field. In the t_{Co} = 0.6 nm samples, the limited diffusion of Ir and Mn atoms in the $Co_{(3)}$ layer explains the very reduced effect of the Pt spacer on the exchange bias effect. In these samples, the disruption of exchange interactions introduced by the Pt spacer between Mn and Co spins has a weaker detrimental influence on the exchange bias field than the benefit produced by the limitation of the Mn and Ir diffusion in the $Co_{(3)}$ layer. The effects of the thickness dependent inter-diffusion on the saturation magnetization, Curie temperature (and correlatively on the exchange stiffness) and interfacial anisotropies were evidenced.

References

[1] Meiklejohn W H and Bean C P 1956 *Phys. Rev.* **102** 1413

[2] Meiklejohn W H and Bean C P 1957 *Phys. Rev.* **105** 904

[3] Nogués J and Schuller I K 1999 *J. Magn. Magn. Mater.* **192** 203

[4] Berkowitz A E and Takano K 1999 *J. Magn. Magn. Mater.* **200** 552

[5] Stamps R L 2000 *J. Phys. D* **33** R247

[6] Kiwi M 2001 *J. Magn. Magn. Mater.* **234** 584

[7] Dieny B, Speriosu V S, Parkin S S P, Gurney B A, Wilhoit D R and Mauri D 1991 *Phys. Rev. B* **43** 1297

[8] Tehrani S, Slaughter J M, Deherrera M, Engel B N, Rizzo N D, Slater J, Durlam M, Dave R W, Janesky J, Butcher B, Smith K and Grynkewich G 2003 *Proc. IEEE* **91** 703

[9] Maat S, Takano K, Parkin S S P and Fullerton E E 2001 *Phys. Rev. Lett.* **87** 087202

[10] Garcia F, Casali G, Auffret S, Rodmacq B and Dieny B 2002 *J. Appl. Phys.* **91** 6905

[11] Marrows C H 2003 *Phys. Rev. B* **68** 012405

[12] Sort J, Dieny B, Fraune M, Koenig C, Lunnebach F, Beschoten B and Guntherodt G 2004 *Appl. Phys. Lett.* **84** 3696

[13] Kagerer B, Binek C, Kleemann W 2000 *J. Magn. Magn. Mater.* **217** 139

[14] Garcia F, Sort J, Rodmacq B, Auffret S and Dieny B 2003 *Appl. Phys. Lett.* **83** 3537

[15] Sort J, Baltz V, Garcia F, Rodmacq B and Dieny B 2005 *Phys. Rev. B* **71** 054411

[16] Hashimoto S, Ochiai Y and Aso K 1989 *J. Appl. Phys.* **66** 4909

[17] Carcia P F 1988 *J. Appl. Phys.* **63** 5066

[18] Kim S S, Hwang J Y and Rhee J R 2007 *J. Magn. Magn. Mater.* **310** 2310

[19] Kim J H and Shin S C 1996 *J. Appl. Phys.* **80** 3121

[20] Garcia F, Fettar F, Auffret S, Rodmacq B and Dieny B 2003 *J. Appl. Phys.* **93** 8397

[21] van Dijken S, Moritz J and Coey J M D 2005 *J. Appl. Phys.* **97** 063907

[22] Sort J, Garcia F, Rodmacq B, Auffret S, and Dieny B 2004 *J. Magn. Magn. Mater.* **272-276** 355

[23] Moritz J, van Dijken S and Coey J M D 2005 *Eur. Phys.* J. B **45** 191

[24] Lechevallier L, Zarefy A, Lardé R, Chiron H, Le Breton J M, Baltz V, Rodmacq B and Dieny B 2009 *Phys. Rev. B* **79** 174434

[25] Larson D J, Petford-Long A K, Ma Y Q and Cerezo A 2004 *Acta Materialia* **52** 2847

[26] Ayon A A, Braff R, Lin C C, Sawin H H and Schmidt M A 1999 *J. Electrochem. Soc.* **146** 339

[27] Gault B, Vurpillot F, Vella A, Gilbert M, Menand A, Blavette D and Deconihout B 2006 *Rev. Sci. Instrum.* **77** 043705

[28] Lardé R, Lechevallier L, Zarefy A, Bostel A, Juraszek J, Le Breton J M, Rodmacq B and Dieny B 2009 *J. Appl. Phys.* **105** 084307

[29] Bas P, Bostel A, Deconihout B and Blavette D 1995 *Appl. Surf. Sci.* **87** 298

[30] Zhou X W, Wadley H N G, Johnson R A, Larson D J, Tabat N, Cerezo A, Petford-Long A K, Smith G D W, Clifton P H, Martens R L and Kelly T F 2001 *Acta Materialia* **49** 4005

[31] Sort J, Dieny B and Nogués J 2005 *Phys. Rev. B* **72** 104412

[32] Bertero G A, Sinclair R, Park C H and Shen Z X 1995 *J. Appl. Phys.* **77** 3953

[33] Metaxas P J, Jamet J P, Mougin A, Cormier M, Ferré J, Baltz V, Rodmacq B, Dieny B and Stamps R L 2007 *Phys. Rev. Lett.* **99** 217208

[34] Bozorth R, "Ferromagnetism", D. Van Nostrand Company Inc., Princeton, New Jersey (1951) p291 and 441

[35] Kittel C, 1946 *Phys. Rev.* **70** 965

[36] Hashimoto S, Ochiai Y and Aso K 1990 *J. Appl. Phys.* **67** 4429

[37] Gehanno V, Samson Y, Marty A, Gilles B and Chamberod A 1997 *J. Magn. Magn. Mater.* **172** 26

[38] Hellwig O, Berger A, Kortright J B and Fullerton E E 2007 *J. Magn. Magn. Mater.* **319** 13

[39] Kaplan B and Gehring G A 1993 *J. Magn. Magn. Mater.* **128** 111

[40] Baltz V, Marty A, Rodmacq B and Dieny B 2007 *Phys. Rev. B* **75** 014406

	t_{Co} = 0.4 nm		t_{Co} = 0.6 nm	
	t_{Pt} = 0 nm	t_{Pt} = 0.4 nm	t_{Pt} = 0 nm	t_{Pt} = 0.4 nm
Saturation magnetization M$_S$ (e.m.u./cm^3) at 300 K				
n = 7	765 ± 39	1025 ± 52	1093 ± 55	1208 ± 61
n = 1	673 ± 34	949 ± 48	1051 ± 53	1100 ± 55
Saturation magnetization M$_S$ (e.m.u./cm^3) at 5 K				
n = 7	1262 ± 63	1474 ± 74	1296 ± 65	1458 ± 73
n = 1	1239 ± 62	1332 ± 67	1261 ± 63	1333 ± 67

Table 1: saturation magnetization M$_S$ values at 5 K and 300 K for t_{Co} = 0.4 and 0.6 nm, t_{Pt} = 0 and 0.4 nm, n = 1 and 7. The uncertainties correspond to an error of 5%.

	t_{Co} = 0.4 nm		t_{Co} = 0.6 nm	
	t_{Pt} = 0 nm	t_{Pt} = 0.4 nm	t_{Pt} = 0 nm	t_{Pt} = 0.4 nm
Exchange bias field values at 300 K (Oe)				
n = 7	12	95	151	55
n = 1	17	115	230	125
Exchange bias field values at 5 K (Oe)				
n = 7	112	141	329	184
n = 1	138	306	434	218

Table 2: exchange bias field values at 5 K and 300 K, for t_{Co} = 0.4 and 0.6 nm, t_{Pt} = 0 and 0.4 nm, n = 1 and 7.

Figure captions

Figure 1. 2D projection of the 3D-reconstruction of an analyzed volume representing the spatial distribution of Pt, Co, Ir and Mn atoms in approximately three sequences of a $[(Pt/Co_{0.6nm})_3/IrMn]_7$ multilayer.

Figure 2. 2D projection of the 3D-reconstruction of one $(Pt/Co_{0.6nm})_3$ sequence in a $[(Pt/Co_{0.6nm})_3/IrMn]_7$ multilayer showing the spatial distribution of Pt atoms. The Pt atomic planes corresponding to the Pt(111) texture are observed in the three Pt layers. The thickness of their crystalline zone is estimated.

Figure 3. 2D projection of the 3D-reconstruction corresponding to the spatial distribution of Co and IrMn atoms in one sequence of a $[(Pt_{2nm}/Co_{0.6nm})_3/Pt_{tPt}/IrMn_{7nm}]$ multilayer for (a) $t_{Pt} = 0$ and (b) $t_{Pt} = 0.4$ nm.

Figure 4. 2D projection of the 3D-reconstruction corresponding to the spatial distribution of Co and IrMn atoms in one sequence of a $[(Pt_{2nm}/Co_{tCo})_3/IrMn_{7nm}]$ multilayer, for (a) $t_{Co} = 0.4$ nm and (b) $t_{Co} = 0.6$ nm.

Figure 5. The Pt, Co and Mn concentration profiles, corresponding to the analyzed volume presented in figure 3 (samples with $t_{Co} = 0.6$ nm), (a) for $t_{Pt} = 0$ nm and (b) for $t_{Pt} = 0.4$ nm. For the sake of clarity, the Ir profile that is connected to the Mn one is not represented. Figures 5 (c) and 5 (d) are enlargements of figures 5 (a) and 5 (b) in the (Pt/Co)/IrMn interface zone, respectively. For the sake of clarity, the Ir profile, which is connected to the Mn one, is not represented.

Figure 6. Pt, Co and Mn concentration profiles corresponding to the (Pt/Co)/IrMn interface zone: for, (a) t_{Co} = 0.4 nm and (b) t_{Co} = 0.6 nm. For the sake of clarity, the Ir profile, which is connected to the Mn one, is not represented.

Figure 7. Typical hysteresis loops of the $[(Pt/Co_{tCo})_3/Pt_{tPt}/IrMn]_n$ multilayers with (t_{Pt} = 0 nm and t_{Pt} = 0.4 nm measured at room temperature, by SQUID magnetometer, the magnetic field being applied perpendicular to the film plane. (Continues line) without Pt spacer and (dashed line) with Pt spacer, for: (a) t_{Co} = 0.4 nm, n = 1, (b) t_{Co} = 0.6 nm, n = 1, (c) t_{Co} = 0.4 nm, n = 7, and (d) t_{Co} = 0.6 nm, n = 7.

Figure 8. Typical hysteresis loops of the $[(Pt/Co_{tCo})_3/Pt_{tPt}/IrMn]_n$ multilayers with (t_{Pt} = 0 nm and t_{Pt} = 0.4 nm measured at 5 K, by SQUID magnetometer, the magnetic field being applied perpendicular to the film plane. (Continues line) without Pt spacer and (dashed line) with Pt spacer, for: (a) t_{Co} = 0.4 nm, n = 1, (b) t_{Co} = 0.6 nm, n = 1, (c) t_{Co} = 0.4 nm, n = 7, and (d) t_{Co} = 0.6 nm, n = 7.
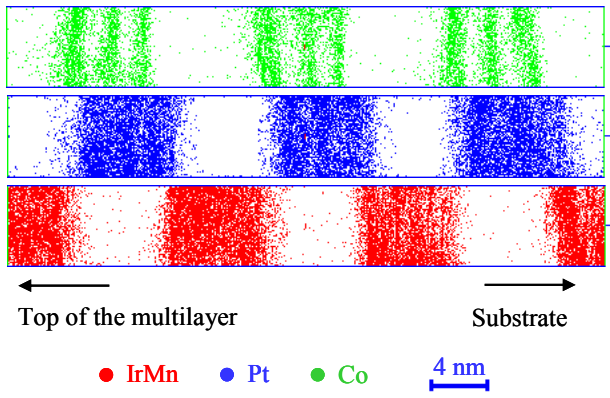
Top of the multilayer   Substrate
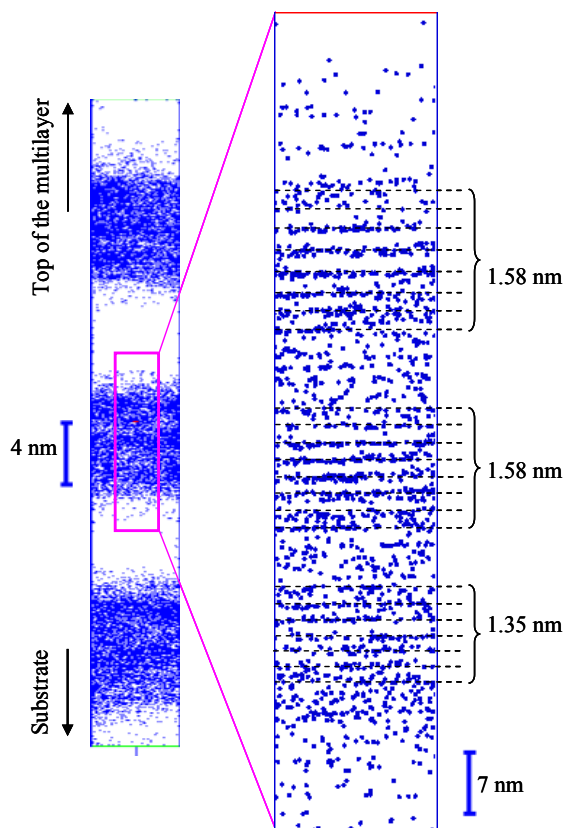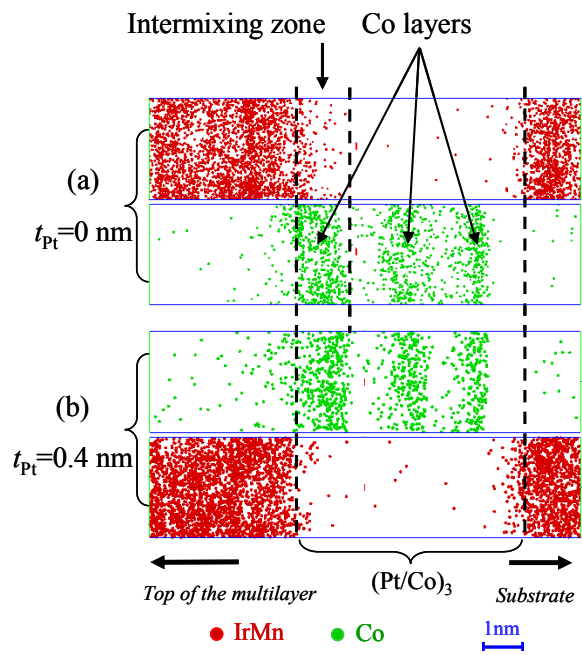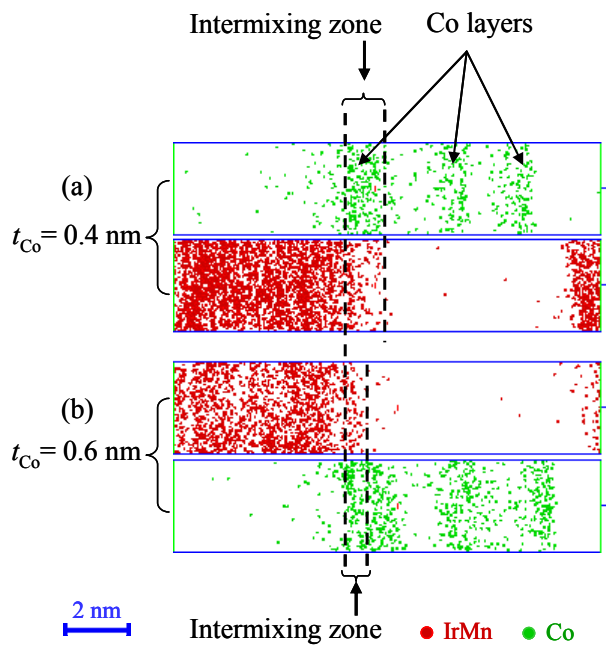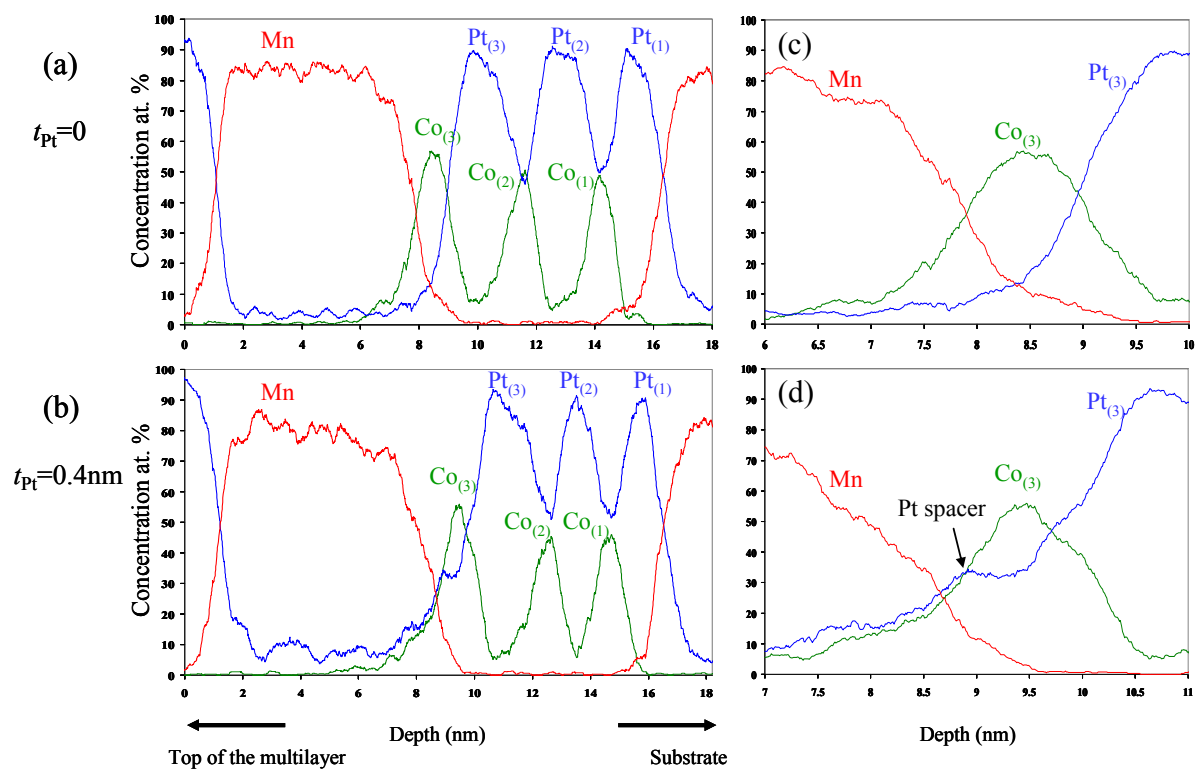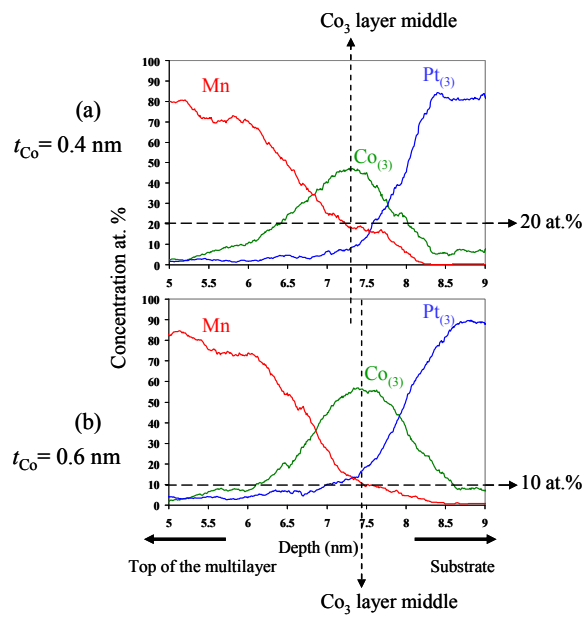
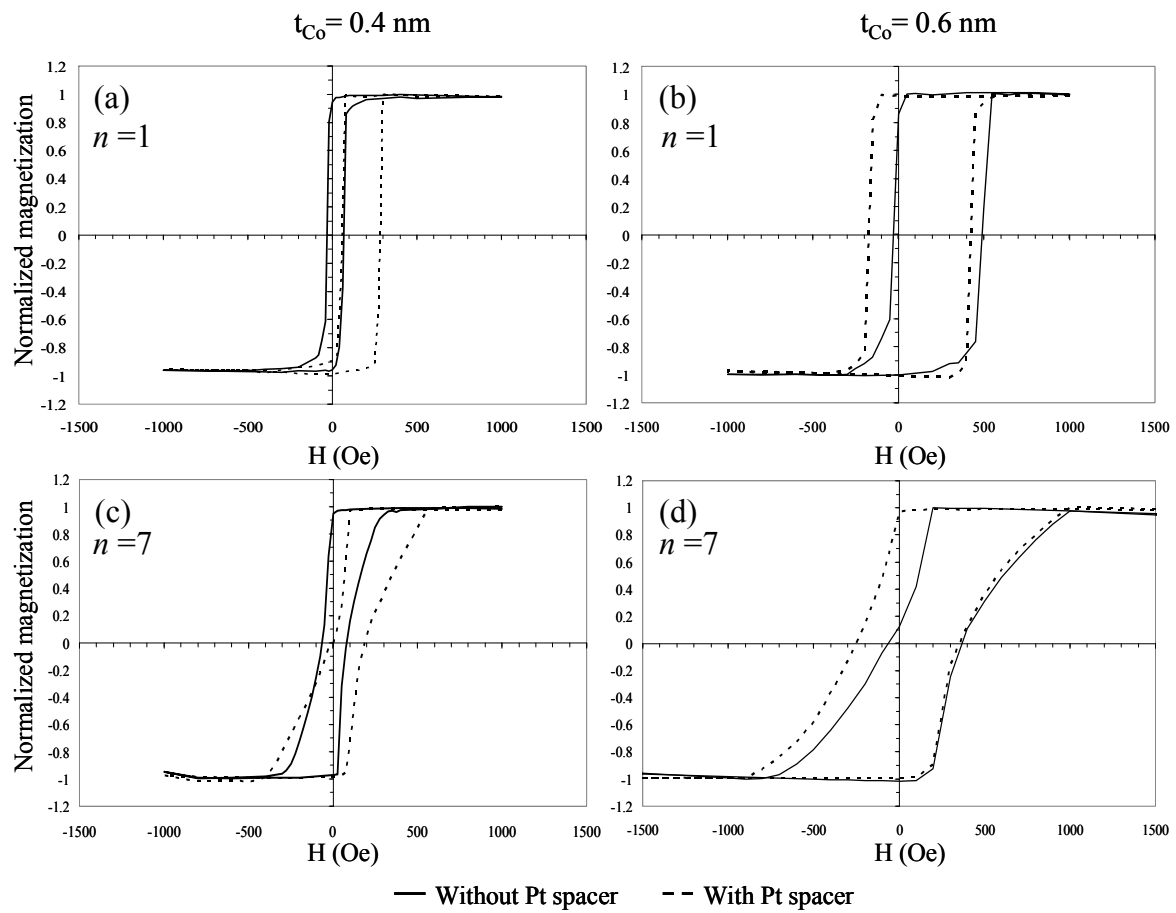● IrMn   ● Pt   ● Co |— 4 nm —|

Figure 1

Figure 2

Figure 3

Figure 4

Figure 5

Figure 6

t_Co = 0.4 nm   t_Co = 0.6 nm

Without Pt spacer   With Pt spacer

Figure 7

Figure 8